Computers and Concrete, Vol. 8, No. 1 (2011) 23-41 23
DOI: http://dx.doi.org/10.12989/cac.2011.8.1.023

Numerical simulation of concrete confined by transverse reinforcement

Zhenhuan Song and Yong Lu*

Institute for Infrastructure and Environment, Joint Institute of Civil and Environmental Engineering, School of Engineering, The University of Edinburgh, The Kings Buildings, Edinburgh, EH9 3JL, UK

(Received January 3, 2010, Accepted February 26, 2010)

Abstract. The behaviour of concrete confined by transverse reinforcement is a classical topic. Numerous studies have been conducted to establish the stress-strain relationships for concrete under various confining reinforcement arrangements. Many empirical and semi-empirical formulas exist. Simplified analytical models have also been proposed to evaluate the increase in the strength and ductility of confined concrete. However, relatively few studies have been conducted to utilise advanced computational models for a realistic simulation of the behaviour of concrete confined by transverse reinforcement. As a matter of fact, high fidelity simulations using the latest numerical solvers in conjunction with advanced material constitutive models can be a powerful means to investigating the mechanisms underlying the confining effects of different reinforcement schemes. This paper presents a study on the use of high fidelity finite element models for the investigation of the behaviour of concrete confined by stirrups, as well as the interpretation of the numerical results. The development of the models is described in detail, and the essential modelling considerations are discussed. The models are then validated by simulating representative experimental studies on short columns with different confining reinforcement schemes. The development and distribution of the confining stress and the subsequent increase in the axial strength are examined. The models are shown to be capable of reproducing the behaviour of the confined concrete realistically, paving a way for systematic parametric studies and investigation into complicated confinement, load combination, and dynamic loading situations.

Keywords: concrete; confinement; transverse reinforcement; numerical simulation; finite element model; confining mechanisms.

1. Introduction

The stress-strain behaviour of confined concrete is different from that of unconfined concrete, and the difference is dependent upon the level of confining stress, which in turn depends on the mechanisms by which the confining stress is developed. In the case of confinement by transverse reinforcement, this involves the amount and configuration of the stirrups. The prediction of stress-strain characteristics in relation to the transverse reinforcement has been a subject of continuous research effort for decades.

A number of empirical or semi-empirical models have been developed to describe the behaviour of axially-loaded RC columns confined by transverse reinforcement based on experimental and simplified theoretical studies, for example Park (1982), Sheikh (1982), Saatcioglu and Razvi (1992).

* Corresponding author, Professor, E-mail: yong.lu@ed.ac.uk

Most of these models are very practical, but are limited to specific cross section shapes and reinforcement arrangements. Some models cover a wider range of concrete member shapes and typical confinement schemes used in practice (e.g., Saatcioglu and Razvi 1992). A commonly adopted approach in these models is to use a confinement effectiveness factor to scale up the uniaxial strength and ductility of plain concrete. Such a factor is considered to be a function of volumetric mechanical ratio of confining steel, section shape, reinforcement arrangement, concrete strength level, etc. A regression analysis is usually applied to establish the detailed relationship from relevant experimental data. However, the extension of these models to more sophisticated sections (such as hollow and I section) and eccentric loading is not straightforward.

Numerical analysis provides a potentially powerful alternative to simplified methods for studying confinement effectiveness. With a suitable numerical model it is possible to study all types of sections and transverse reinforcement arrangements, and under a variety of static and dynamic loads. With the advancement of the computer power and the computational techniques, an increasing number of modelling studies using finite element methods have emerged in recent years. The main interest of many such studies has been placed on the development of the constitutive models for the concrete material (Liu and Foster 2000, Kwon and Spacone 2002). Some numerical studies were carried out to investigate the effectiveness of certain confinement arrangements in special structural member designs (e.g., Faria *et al*. 2004, Papanikolaou and Kappos 2009).

In this paper, we present a high fidelity numerical simulation model for analyzing the behaviour of concrete confined by transverse reinforcement. The model is developed using a general purpose transient dynamic analysis code, LS-DYNA (2007), and the constitutive models for the materials have pressure and strain-rate sensitive features, thus the model can be used for both quasi-static and dynamic loading analysis, and it can also accommodate any load combinations, for example axial load and bending. In the present paper, we shall concentrate on the demonstration and validation of the basic model, and establish a framework for the interpretation of the numerical results concerning the confinement effect. For this purpose, we choose to simulate axially loaded short columns under static loading, for which experimental data and empirical models are widely available. The axial stress-strain characteristics are compared with the empirical predictions. The effectiveness of different transverse reinforcement schemes is examined, and the detailed process of development of the confining stress and its distribution at different loading stages are illustrated and discussed.

2. A brief review of representative simplified models

Many researchers have proposed analytical models to predict the behaviour of confined concrete and the effectiveness of transverse confining reinforcement. Some representative studies, which are selected for the comparison with the present numerical modelling study, are summarised below.

Early research on the behaviour of confined concrete focused on the enhancement of the ductility due to the presence of the transverse reinforcement (e.g., Kent and Park 1971). Park *et al*. (1982) later proposed a modified model which takes into account the enhancement in the concrete strength and the peak strain due to confinement. Sheikh and Uzumeri (1982) introduced the concept of effectively confined area to measure the confinement effect with different transverse reinforcement arrangements, and proposed a confinement effectiveness coefficient which is a function of the distribution of longitudinal steel bars, and the configuration and spacing of the stirrups.

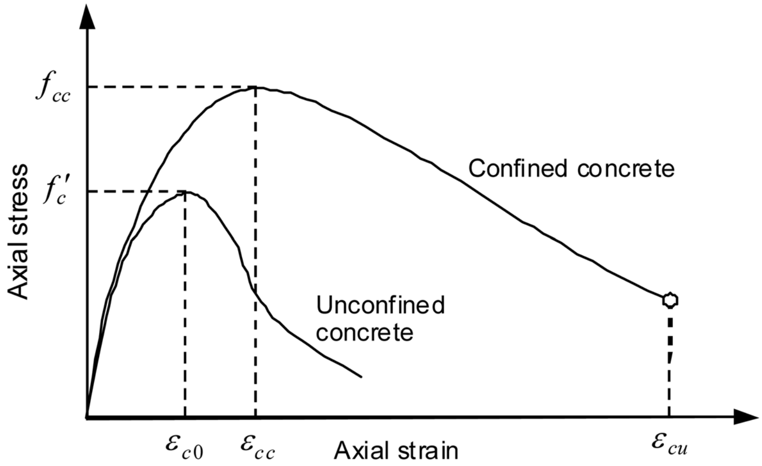

Fig. 1 Schematic of the stress-strain curves for unconfined and confined concrete

Mander *et al.* (1988) presented a unified model of confined concrete, whereby the influence of various types of confinement is taken into account by introducing an effective lateral confining stress, which depends on the arrangements of the transverse and longitudinal reinforcement. Along a similar line of relating to the confining stress, Saatcioglu and Razvi (1992) studied the confined concrete strength and ductility through the lateral confinement pressure. The model is based on the calculation of equivalent uniform confinement pressure resulting from different arrangements of reinforcement cages.

For a general comparison of different models, herein we refer to the governing parameters in the axial compressive stress-strain curves for unconfined and confined concrete as shown in Fig. 1, namely the strength of unconfined concrete, f_c'; the strength of confined concrete, f_{cc}; the strain at the maximum stress of unconfined concrete, ε_{co}; the strain at the maximum stress of confined concrete, ε_{cc}; and the ultimate strain of the confined concrete, ε_{cu}. The effectiveness of the confinement may be measured by

a) the strength enhancement factor, K_s

$$K_s = \frac{f_{cc}}{f_c'} \tag{1}$$

b) the ratio of the strain at the peak stress of confined to unconfined concrete, K_d

$$K_d = \frac{\varepsilon_{cc}}{\varepsilon_{c0}} \tag{2}$$

c) the ultimate strain of the confined concrete, ε_{cu}.

Among these factors, the strength enhancement factor K_s is most straightforward and easy to determine from an experiment. K_d is also well defined, although its measurement may not be as accurate as K_s. On the other hand, the exact definition of the ultimate strain differs in different studies, although the general concept is similar. In the present study, we shall mainly use the K_s factor in the comparison of the numerical and experimental results. A summary of the various formulas proposed by different researchers for K_s, along with K_d, is given in Table 1.

Table 1 Summary of expressions of strength and strain enhancement factors (refer to the source publications for detailed definitions of the variables)

Source	$K_s = \frac{f_{cc}}{f_c'}$	$K_d = \frac{\varepsilon_{cc}}{\varepsilon_{co}}$
Park *et al.*(1982)	$1.0 + \frac{\rho_w f_y}{f_c'}$	$1.0 + \frac{\rho_w f_y}{f_c'}$
Sheikh and Uzumeri (1982)	$1 + \frac{b_c^2}{140 P_{occ}}\left[\left(1 - \frac{nC^2}{5.5 b_c^2}\right)\left(1 - \frac{s}{2b_c}\right)\right]$	$1 + \frac{248}{C}\left[1 - 5.0\left(\frac{s}{B}\right)^2\right]\frac{\rho_w f_y}{f_c'}$
Mander *et al.* (1988)	$-1.254 + 2.254\sqrt{1 + 7.94\frac{f_l'}{f_c'}} - 2\frac{f_l'}{f_c'}$	$1 + 5\left[\frac{f_{cc}'}{f_c'} - 1\right]$
Saatcioglu and Razvi (1992)	$1 + k_1\frac{f_{le}}{f_c'}$	$1 + 5k_1\frac{f_{le}}{f_c'}$

3. Numerical model

3.1 Basic model configuration

Rectangular (including square) and circular sections are two typical section shapes used in structural design for axially loaded members (columns), and so most of the experimental studies on concrete confined by transverse reinforcement have been conducted on specimens having a rectangular or a circular section. In the present study, two square sections and one circular section are selected for the modelling of confined concrete in a short column setting. Fig. 2 shows the schematic of the cross-sections and the reinforcement arrangements. To enable a direct comparison of the numerical results with available experimental data, the section of the square specimen is chosen to be 200 × 200 mm, and the length is 600 mm. The diameter of the circular specimen is also 200 mm, with the same length as the square specimens. The concrete cover is set to be 15 mm in all specimens. The spacing between the stirrups is initially set to 80 mm.

The computational finite element model follows closely the geometry and reinforcement arrangements of the actual short-column specimens, using brick elements for both concrete and steel bars. Considering the symmetry of the specimens under an idealized condition, only one-eighth of each

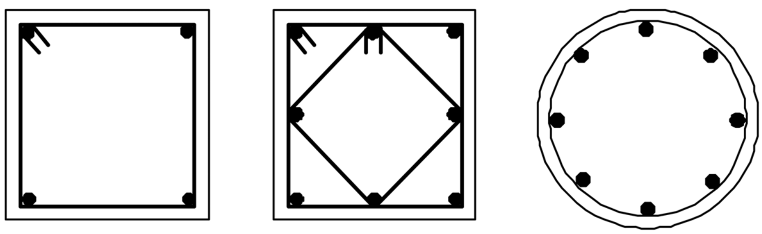

Fig. 2 Schematic of cross-section and reinforcement arrangements in the numerical simulation

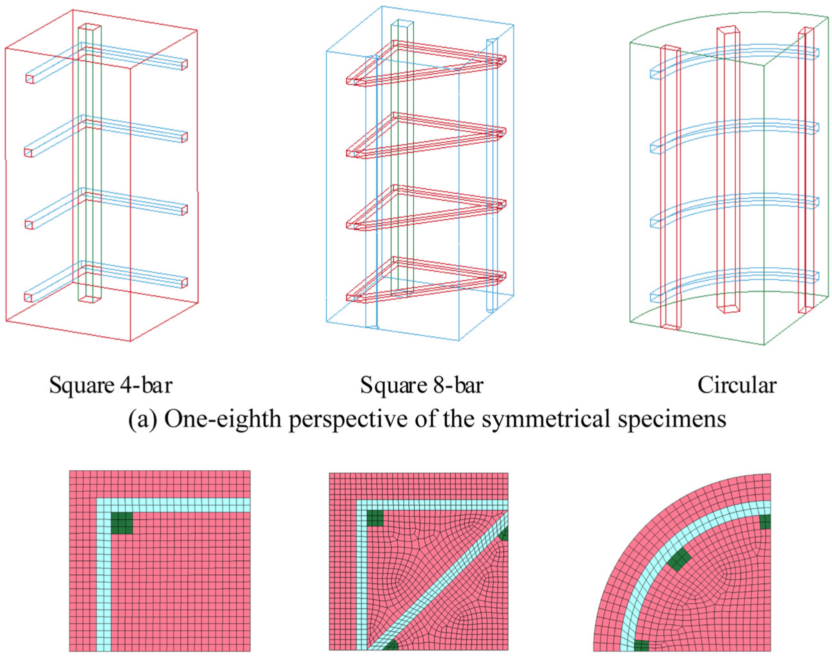

(a) One-eighth perspective of the symmetrical specimens

(b) Finite element mesh of the cross sections

Fig. 3 Illustration of the finite element model configurations

short-column specimen needs to be modelled, as illustrated in Fig. 3(a). For simplicity, the steel bars are modelled to have a square section with approximately the same section area as the actual round bars, and the interface between the rebar surface and the concrete is assumed to be perfectly bonded. These simplifications are deemed to be reasonable for the current problem concerning the confinement effect on the concrete, which is mainly derived from the pressure for which the steel-rebar interface behaviour is expected to play a minimal role.

In the 4-bar square specimen, the cross-section area of the transverse steel is set to 8 × 8 mm, and that of the longitudinal bar is 12 × 12 mm, equivalent to a round section of diameter 9 mm and 13.5 mm, respectively. For a comparison purpose, the same volumetric ratio is maintained in the 8-bar square and the circular column specimens; thus, the cross-section of the transverse steel becomes 6 × 6 mm per leg in the 8-bar square column, and 8 × 8 mm in the circular column. The final volumetric ratio of the transverse reinforcement in all specimens is 1.33~1.38%, and that of the longitudinal reinforcement is 1.41~1.50%. Trial analyses indicate that a nominal mesh grid size of 3-4 mm is suitable for all the models.

The concrete considered in this study has an unconfined compressive strength (cylinder) 30 MPa, f_c'. The steel bar is modelled as a piecewise elasto-plastic material. The longitudinal steel rebar has yield strength 460 MPa, and the transverse reinforcement has yield strength 250 MPa. They both have a Young's modulus of 210 GPa. The strain hardening branch is governed by a tangent modulus chosen to be 0.5% of their Young's modulus.

The transient explicit finite element analysis code LS-DYNA (v971) is used to perform the analysis. The uniaxial loading is imposed with a smoothed displacement boundary time history, at a rate which is sufficiently slow (< 0.1/s) to avoid any oscillation and dynamic effects. The same model can be used to conduct analysis under high rate loading to evaluate the dynamic and strain rate effect on the concrete confined by reinforcement cages. This is partly the reason for the choice of using LS-DYNA and an explicit time integration scheme for the computation in the present study, so that extension to the analysis in the dynamic loading regime is straightforward. As an illustrative example, an example of dynamic analysis on a short column is given in the last part of the paper.

3.2 Concrete material model

The soundness of the concrete material constitutive model is essential in a numerical analysis of the behaviour of concrete under a passive confinement by reinforcement cages. Important considerations include the pressure dependency and the lode angle dependency of the strength surfaces, and rate dependency for dynamic analysis, among others. In the transient dynamic analysis realm, Tu and Lu (2009) reviewed a range of possible concrete material models, including several sophisticated models with comprehensive capabilities.

One of such comprehensive concrete material models is the so-called Concrete Damage Model (or K&C model) developed by Malvar *et al.* (1997, 1999). This material model evolved from the early version used in DYNA3D finite element program. The latest version of the model (release III) is now available in LS-DYNA as material #72R3. The model uncouples the total stress into an isotropic and a deviatoric part. The isotropic behaviour is controlled by a compaction curve relating the current pressure to the current and previous compressive volumetric strain, and the deviatoric stress is defined as a linear combination of failure surfaces based on a three-invariant formulation. Fig. 4 depicts the compaction curve, and the three strength surfaces, namely an initial yield surface, a maximum failure surface and a residual surface. The general strength criterion is given by a uniform expression as

$$\Delta\sigma = \sqrt{3J_2} = f(p, J_2, J_3) \tag{3}$$

where $\Delta\sigma$ and p denote the principal stress difference and pressure, respectively. I_1, J_2 and J_3 are the stress invariants. In the principal stress space, the meridian of the strength surface is governed by $f(p,J_2,J_3) = \Delta\sigma^c \times r'$, where $\Delta\sigma^c$ represents the compressive meridian and r' is a function of the Lode angle. The compressive meridians of the three strength surfaces have a similar form as:

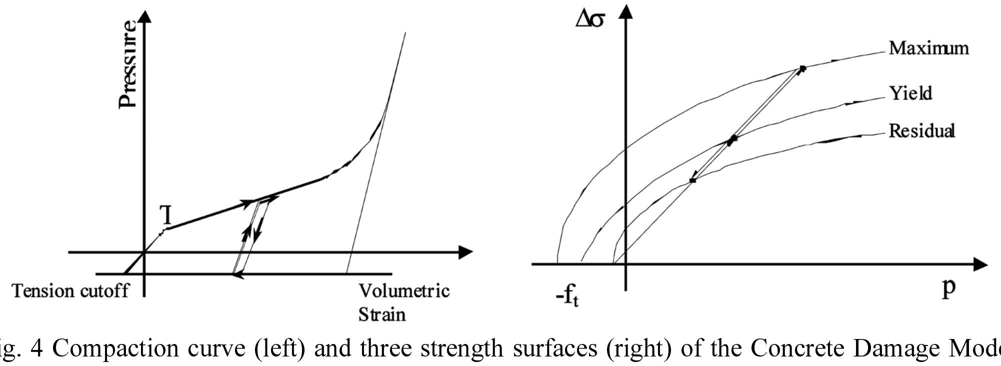

Fig. 4 Compaction curve (left) and three strength surfaces (right) of the Concrete Damage Model

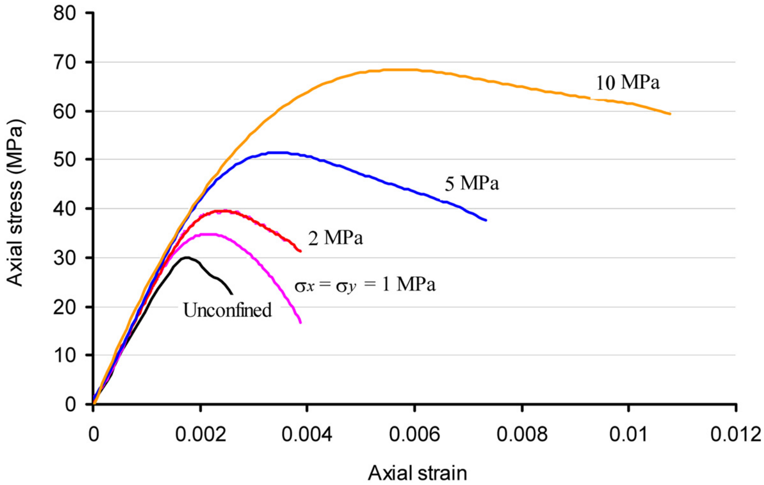

Fig. 5 Single-element analysis of the axial compressive stress-strain relationship under different levels of active confining stresses

$$\Delta\sigma = a_0 + \frac{p}{a_1 + a_2 p} \tag{4}$$

where a_0, a_1 and a_2 are free parameters. For the failure surface, $a_0 = 0$. Thus, for the three failure surfaces eight free parameters need be determined, based on experimental data. Extensive calibration studies exist in relation to the determination of these parameters (e.g., Malvar *et al.* 1997, Tu and Lu 2009), and for typical classes of concrete, these parameters may be generated automatically within LS-DYNA.

The loading path after yield is defined by interpolation between the respective strength surfaces. The development of nonlinearity is controlled by a variable called yield scale factor η, which in turn is determined by a damage function λ. Different damage evolution in tension and compression is realized by different definitions of the λ function. Again, for typical classes of concrete, recommended specifications of these parameters can be found from relevant literature (e.g., Malvar *et al.* 1997).

In order to verify the pressure dependency of the above concrete material model in reproducing the anticipated increase of the strength and ductility under a triaxial compression condition, the single element approach is used, in which a single finite element is subjected to axial compression with different levels of actively imposed lateral confining stresses. Fig. 5 shows the achieved axial compressive stress-strain curves for 30-MPa concrete under four different levels of the confining stresses, namely 1, 2, 5 and 10 MPa, respectively. It can be observed that the achieved compressive strength and the ductility increase with the increase of the lateral confining stress. The trend is consistent with general experimental observations. More detailed comparison with experimental data will be provided later in the simulation of the passive confinement by transverse reinforcement.

4. Verification of the overall numerical model with experimental data

The numerical model for concrete confined by the steel reinforcement cages is verified by comparing the axial stress-strain curves with relevant experimental results. The square specimen with 8-bar reinforcement

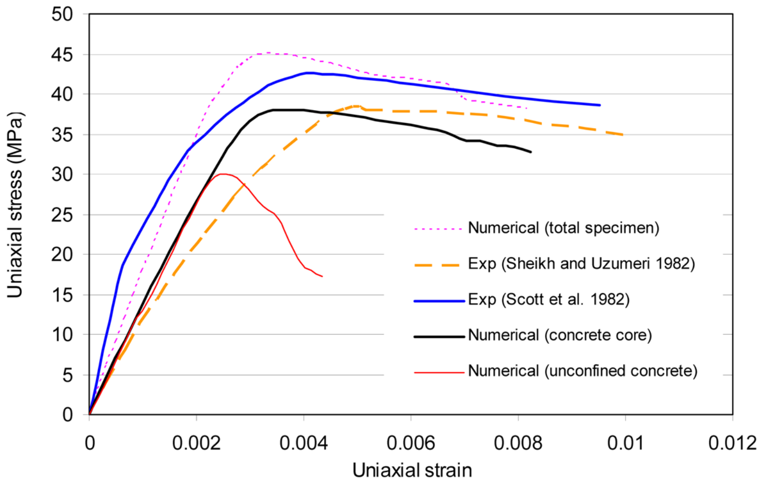

Fig. 6 Comparison of numerical and experimental stress-strain curves

configuration is chosen for this comparison. The corresponding experimental data are extracted from those conducted by Sheikh and Uzumeri (1980) and Scott *et al.* (1982). The test specimens had a similar class of concrete with unconfined compressive strength of 30-40 MPa, but a varying amount of reinforcement, with transverse reinforcement spacing in a range of 30-75 mm, and longitudinal and transverse steel volumetric ratios varying in a range of 1~2.4% and 2.2~4.3%, respectively. Thus the numerical models in the current settings may be regarded as representing the lower bound of the experimental cases.

It should be mentioned that in both numerical and experimental data, the direct contribution of the longitudinal reinforcement in the axial resistance is taken away by subtracting the total applied axial load by the axial forces incurred in the longitudinal steel rebars. Thus the stresses in the concrete are comparable concerning the confining effect, irrespective of the variation in the amount of the longitudinal reinforcement. Further extraction of the concrete stresses within the confined core may be done by taking away the load (stress) within the concrete cover. In the numerical results, both the stresses within the confined core and in the concrete cover are obtained. The total stress including the contribution of the longitudinal steel is also retained for an indicative purpose.

Fig. 6 shows the comparison of numerical and experimental stress-strain curves for the 8-bar configuration. The numerical results resemble quite well the characteristics of the experimental curves, considering the level of disparity that exists among the experimental results. The increase in the strength and the strain at the peak stress as well as the increase in the overall ductility agree favourably with the experimental results. Further validation of the numerical model will be discussed later when comparing the numerical results with relevant empirical predictions.

5. Numerical simulation of three different specimen configurations

Numerical simulation analysis is performed for the three different confinement arrangements shown in Figs. 2 and 3. The results are presented in detail in this section. It should be noted that herein the concrete core is taken as the region bounded by the hoops and the longitudinal bars, while the remaining region is attributed to the concrete cover. The stresses for the whole specimen,

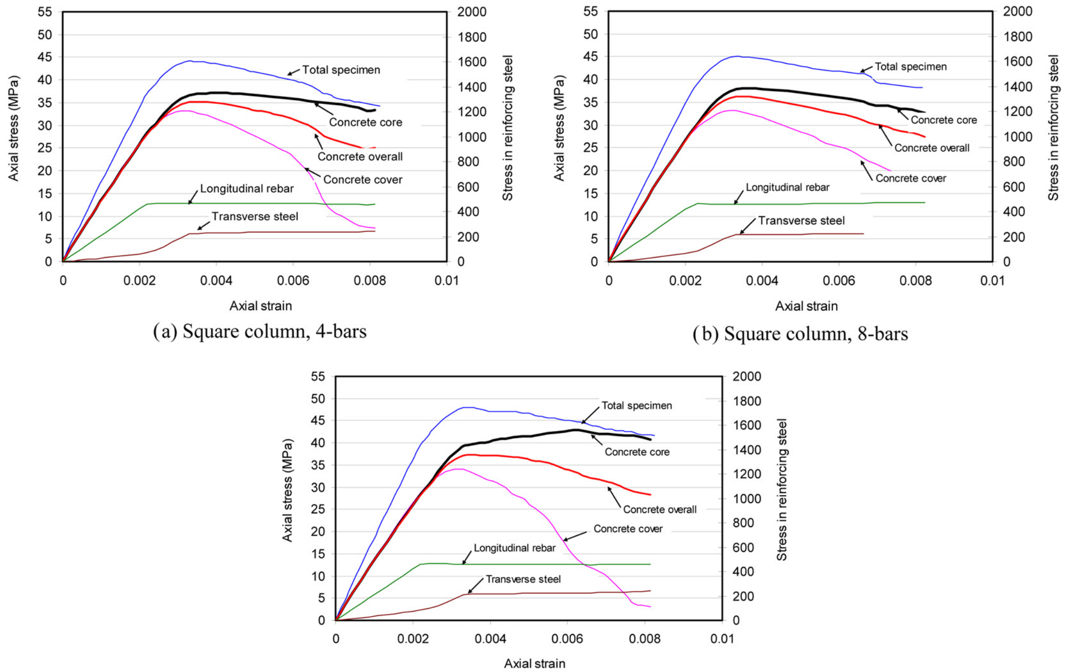

(a) Square column, 4-bars

(b) Square column, 8-bars

(c) Circular column

Fig. 7 Axial stress-strain curves for three specimens

confined core, or cover regions, as indicated in Fig. 7, refer to the average stress among all concrete elements in the respective regions.

5.1 Stress-strain curves

Fig. 7 shows the axial stress-strain curves in the three models. The thick lines are the axial stress-strain curves for the concrete within the confined core, thus may be regarded as representing the confinement effect in the three cases. The remaining curves include the total stress-strain curves (including the contribution of the longitudinal reinforcement), the average stresses within the overall concrete area (including concrete core and cover), and the stresses within the concrete cover, respectively. Besides, the stresses in the longitudinal and transverse steel bars as the axial strain increases are also shown in the figure. By tracking the stress in the transverse reinforcement, one can clearly observe the process of the lateral expansion of the specimens and hence the development of the lateral confining stresses.

As can be observed from the graphs, the total stress and the stress in the confined concrete core reach the peak stress (strength) almost at the same time as the transverse reinforcement reaches its yield strength. This may be explained by the fact that, up to this stage the confining stress increases continuously, while the accumulation of damage, which evolves independently from the confinement as the strain increases, remains to be relatively small.

Beyond the first peak stress, the stress-strain curves in the confined concrete core show an apparently increased ductility (or reduced softening rate) in all the specimens, whereas the stress in the concrete cover drops abruptly. The increase in the peak strength and the strain at the peak stress

Table 2 Comparison of strength enhancement between numerical and analytical results

Specimen	*Ks* (Numerical, overall)	*Ks* (Numerical, core)	Park *et al.* (1982)	Sheikh & Uzumeri (1982)	Mander *et al.* (1988)	Saatcioglu & Razvi (1992)
4-bar square	1.17	1.23	1.12	1.20	1.25	1.25
8-bar square	1.21	1.34	1.11	1.28	1.26	1.30
Circular	1.24	1.43	1.12	1.33	1.31	1.35

in the confined concrete core appears to be larger in the 8-bar specimen as compared to the 4-bar specimen, while the circular column exhibits the best performance among the three cases.

A further comparison of the confinement effect in terms of the strength enhancement among the three specimens, and between the numerical analysis and empirical predictions is presented in Table 2. Two strength enhancement factors are calculated from the numerical results, based respectively on the strength within the confined core and the average strength for the whole concrete area (core and cover). The empirical results are calculated using the formulas proposed by four different research groups (shown in the table), respectively.

From the comparison it can be seen that the numerical results agree favourably with the predictions from most of these analytical/empirical models. The numerical results for the confined concrete core tend to be slightly higher than the predictions, and this may be attributed to the fact that in the numerical model the concrete cover does not physically spall even after failure, and this may contribute slightly to the confining effect on the concrete in the core area.

5.2 Confining stress distribution over a cross-section

The confining effect actually depends upon the magnitude as well as the distribution of the confining stress. It is physically understood that higher-magnitude and more uniformly distributed confining stress will result in a better confining effect, and vice versa. The numerical simulation results enable a detailed look at these underlying aspects of the overall confining effect. The magnitude and distribution of the confining stress may be examined over different cross-sections and along the height of the specimen.

Fig. 8 and Fig. 9 plot the contours of the confining stress over two cross-sections, namely in the middle between two adjacent stirrups, and at the location where a stirrup is present. The fringe level is set to the magnitude of stress in MPa. Blue (see the PDF version for the coloured plots) indicates the highest compressive stress, i.e., 5 MPa in Fig. 8 and 8 MPa in Fig. 9, while red indicates virtually a neutral (zero) confining stress. The second principal stress is chosen for the illustration, which presents the higher absolute confining stress in the two lateral directions. The contours corresponding to two response levels, one at about the peak stress, and another on the descending branch, are presented.

From the confining stress contour plots, the following observations may be made:

1) The distribution of the confining stress shows a pattern closely related to the configuration of the stirrups. For the square columns, higher confining stress occurs at the corner regions of the stirrups, and in the direction along the sides of the stirrups. Both the magnitude and uniformity of the confining stress are higher in the 8-bar square column than in the 4-bar square column. The circular column exhibits a rather uniform distribution of the confining stress within the confined core.

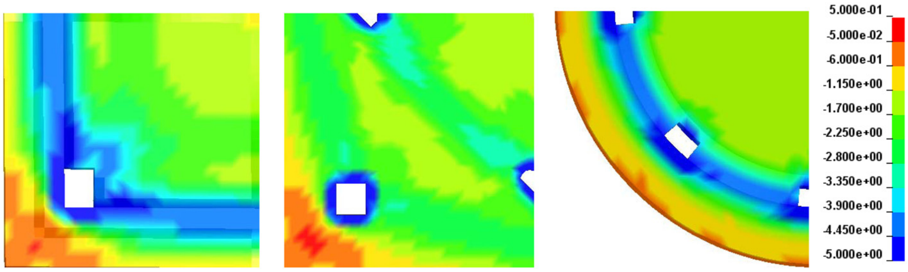

(a) Axial strain = 0.003

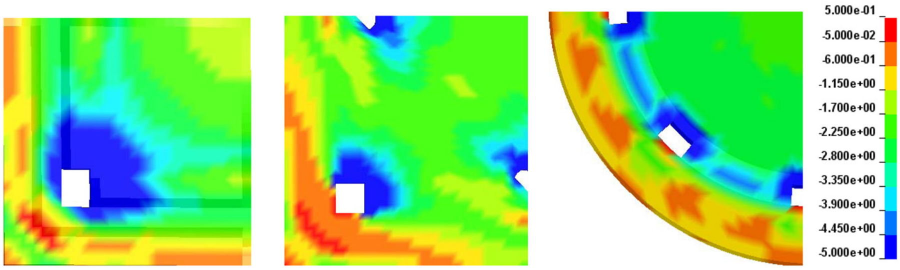

(b) Axial strain = 0.005

Fig. 8 Contours of confining stress over a cross-section between two adjacent stirrups in the three specimens

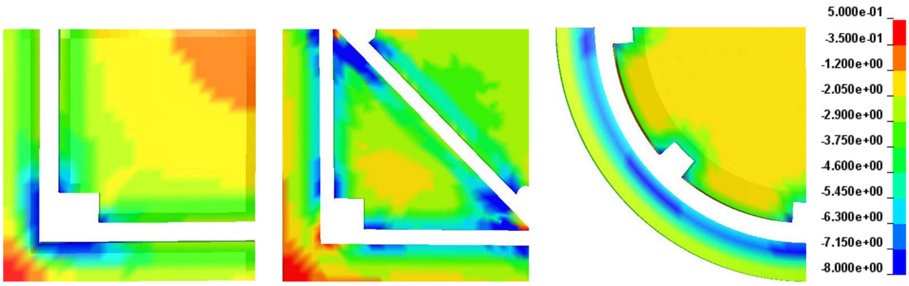

(a) Axial strain = 0.003

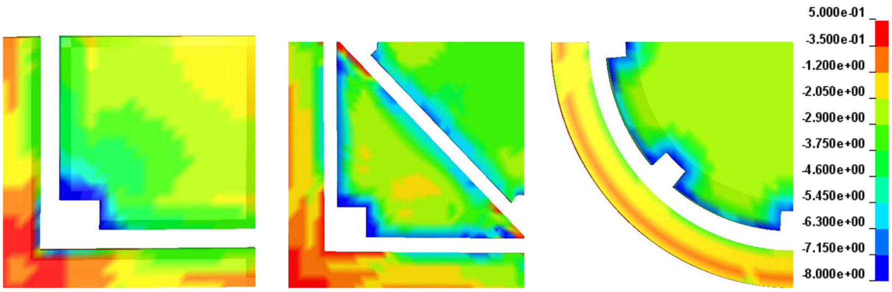

(b) Axial strain = 0.005

Fig. 9 Contours of confining stress at the stirrup section in the three specimens

2) The magnitude of the confining stress is generally higher at the cross-section where the stirrup is located than the cross-section in-between two adjacent stirrups. Taking the circular column

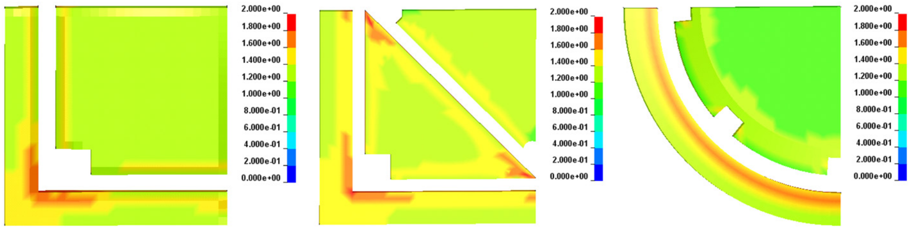

(a) Axial strain = 0.003

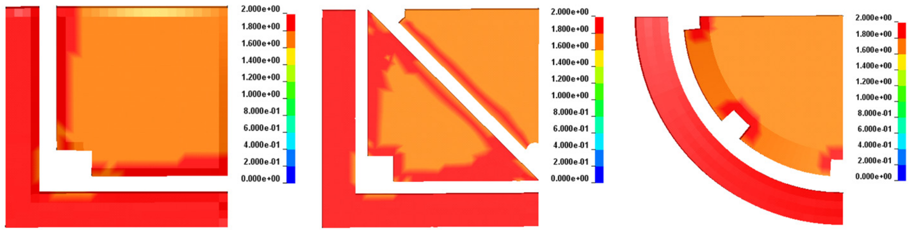

(b) Axial strain = 0.005

Fig. 10 Accumulation of concrete damage in the three specimens

as an example, the confining stress at the stirrup section is about 20% higher than that at the middle section between two stirrups, bearing in mind that in the current numerical model the spacing of the stirrups is 80 mm. The difference is expected to vary if the spacing of the stirrups varies.

3) In all specimens, the magnitude of the confining stress in the confined core tends to further increase after the peak stress is reached. This may be attributed to the continued expansion of the concrete in the lateral direction, in conjunction with the hardening of the stirrups.

As mentioned earlier, despite some further increase in the confining stress, after reaching the peak axial stress the (shear) strength of the concrete material deteriorates at a higher rate, and this leads to the combined outcome of the overall softening of the confined concrete. The rate of softening manifests the effectiveness of the confinement. Fig. 10 depicts the accumulation of the material damage. The damage defined here is a normalized index equal to $2\lambda/(\lambda + \lambda_m)$, where λ_m is the value of damage function (refer to Section 3.2) at the maximum strength. For the damage state between reaching maximum strength and the final failure, the index varies in a range of 1.0-2.0.

It can be observed from Fig. 10 that, at around the peak load level (corresponding to axial strain 0.003), part of the concrete cover has reached the failure state, while the confined concrete core already develops into the inelastic stage, especially in the square columns. At the axial strain of 0.005, the entire concrete cover in all three specimens has failed, and the confined area also reaches a high level of damage.

5.3 Confining stress distribution along height

Another perspective of the uniformity of the confining stress can be obtained by viewing the confining stress contours in the vertical plane. Fig. 11 shows the contours of the confining stress along the height taken from a cut near the symmetric plane of the specimens. For the 8-bar square and the circular specimens, the cut plane is slightly shifted to avoid the longitudinal rebar. The contours at two response levels are plotted, corresponding respectively to an axial strain of 0.003 (about the peak stress level) and 0.005 (post-peak).

The contours exhibit clearly the variation of the distribution of the confining stress over the vertical plane, especially the radiating patterns of the confining effect from the position of the reinforcement to the adjacent areas. It is also noteworthy that, within the confined area the most significant variation of the confining stress is primarily limited to the outer region of the confined core, while in the rest (majority) of the central area the distribution of the confining stress is rather uniform across different sections.

From the contours it can also be observed some arching patterns, running at about 45°, between the layers of the stirrups, with higher confining stress along a zigzag path. These detailed distributions are deemed to be attributable to the interaction between the steel bars and concrete, and they may induce certain effect on the spalling of concrete in the cover and the outer region of the confined area. However, the accuracy of the numerical results at this level of detail could be sensitive to the concrete-steel interface modelling, which is not the primary concern of this paper. In this regard, further investigation is required in future studies.

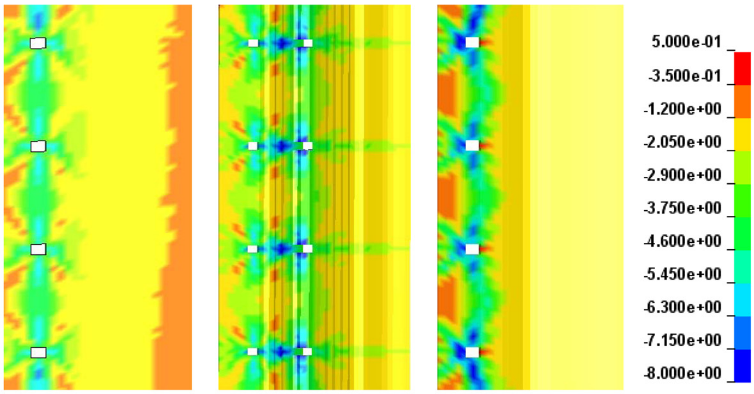

(a) Axial strain = 0.003

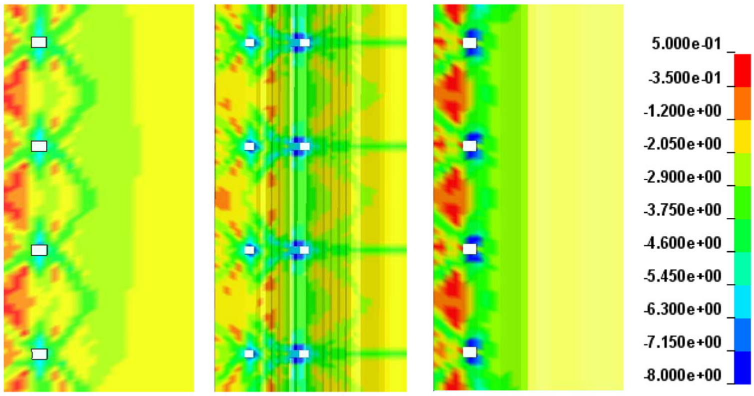

(b) Axial strain = 0.005

Fig. 11 Confining stress distribution along height, left = 4-bar square column, middle = 8-bar square column, right = circular column

5.4 Discussion on the concrete cover spalling-off

Experimental observations indicate that the unconfined concrete cover tends to spall off from the confined concrete core at a relatively low level of axial strain. This effect may be attributed to high tensile strain that develops along the cover-core interface due to Passion's ratio and the presence of the transverse reinforcement (Foster *et al.* 1998). In fact, such an effect can also be observed from the contours of the confining stress shown in Fig. 11, in which the second principal stress exhibits an apparent concentration along the cover-core interface, indicating higher expansion in the lateral direction along the interface path.

In a numerical analysis using FE model, it is possible to eliminate completely the contribution of the concrete cover when it is deemed to have reached the spalling threshold, using for example an element erosion (removal) scheme which is available in many FE codes, or a pre-defined cut-off of stiffness in the constitutive law. However, the determination of the erosion or stiffness cut-off criteria can be a difficult subject, due to its perceivable dependency on the stress condition. On the other hand, without a spalling scheme in place, the failed elements in the concrete cover will still retain certain residual compressive strength, as can be seen from Fig. 7 and also observed in some other numerical studies (Papanikolaou and Kappos 2009). This can cause an overestimation of the overall strength in the specimen and contribute in additional confinement on the concrete core, leading potentially to some inaccurate interpretation of the confining effect from the transverse reinforcement. Such a modelling aspect deserves a further investigation in the future when a more quantitative parametric study is to be carried out.

6. Further evaluation of confining stress

In essence, the confining effect on concrete is realized through the pressure arising from whatever confining mechanism that is put in place. In the case of passive confinement by the transverse reinforcement (or more precisely the reinforcement cage formed by transverse and longitudinal steel bars), the effectiveness of the confinement can be more clearly understood by looking at how the

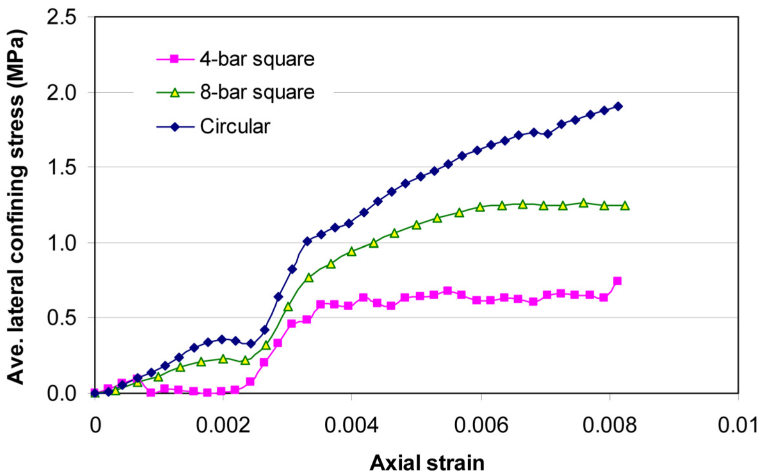

Fig. 12 Development of (passive) confining stress with increase of axial deformation

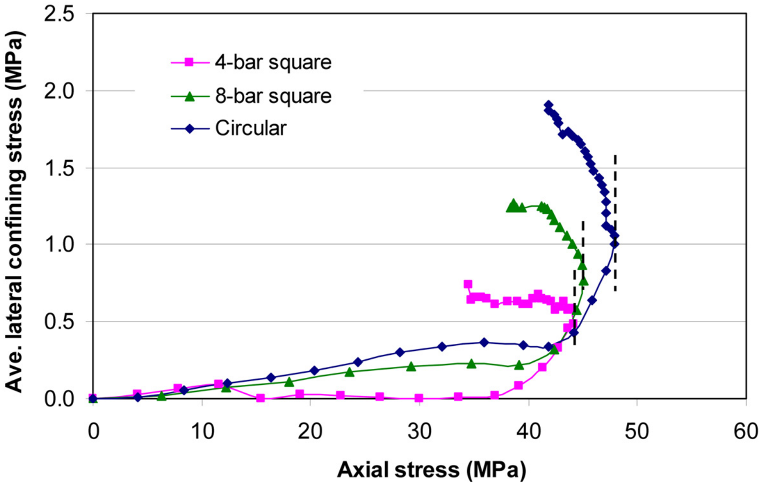

Fig. 13 Development of confining stress vs. axial stress

lateral confining pressure evolves during the course of the response to the axial loading. This section presents a comparative evaluation of the relationship between the axial loading (axial stress/strain) and the lateral confining pressure in the three specimens under consideration.

For this evaluation, the lateral pressure is calculated as the average lateral stress in all elements within the confined area, i.e.

$$\sigma_{conf} = \frac{\sigma_x + \sigma_y}{2} \tag{5}$$

Fig. 12 shows the relationship between the average lateral confining stress and the axial (z-direction) strain for all the three specimens. Note that the peak stress for the confined core occurs at an axial strain around 0.0035. Fig. 13 plots the relationship between the average confining stress and the axial stress to provide another perspective about the development of the confining stress and its effect on the axial resistance before and after the peak axial load.

Based on these figures, the evolution of the (passive) confining stress due to the transverse reinforcement may be divided into three stages, namely a pre-unconfined peak stress stage (stage 1), which is up to about an axial strain of 0.002; a transition stage up to the peak stress of the confined concrete (stage 2); and post-confined peak stress or softening stage (stage 3). In conjunction with Fig. 7, it can be found that these three stages correlate well with three stages of the development of the stress in the transverse reinforcement, respectively. At stage 1, the increase of the confining stress as well as the stress in the transverse reinforcement is gradual and at a lower rate. This is explicable since the concrete expands at a slow rate (smaller Poisson’s ratio) before reaching the peak stress of the unconfined concrete. A rapid increase of the confining stress follows (stage 2), due apparently to the plastic deformation of the concrete material. The confining stress appears to continue increase at stage 3, especially in the 8-bar square and circular columns, but at a reduced rate. The continued increase at this stage may be attributed to the hardening of the transverse reinforcement and re-distribution of the stresses within the confined area.

It is worth noting that in the 4-bar square column, the increase of the confining stress mainly incur at stage 2, whereas the increase at stage 1 and stage 3 are minimal. This further signifies the relatively less satisfactory confining effect in such a transverse reinforcement configuration.

From Fig. 13, it can also be clearly observed that the peak axial stress (strength) of the confined concrete correlates closely with the magnitude of the confining stress when the peak stress is attained.

CEB-FIP 1990 (1993) recommended a generic confinement efficiency curve regarding the maximum strength and the “effective lateral stress”, and it takes into account the non-uniformity of distribution of confining stress. The linearized approximation of the confined concrete strength is given by the following expression

$$f^*_{cc} = f_{cc}(1.000 + 2.50\alpha\omega_\omega) \quad \text{for} \quad \sigma_2/f_{cc} < 0.05 \tag{6}$$

$$f^*_{cc} = f_{cc}(1.125 + 1.25\alpha\omega_\omega) \quad \text{for} \quad \sigma_2/f_{cc} > 0.05 \tag{7}$$

where f_{cc} is unconfined compressive strength, σ_2 is lateral stress, and ω_ω denotes the volumetric mechanical ratio of confining steel. $\alpha = \alpha_n\alpha_s$ is a coefficient related to the stirrup (hoop) patterns, with α_n and α_s being the reduction factors in terms of the effective confined area in the lateral direction (depending on hoop pattern) and elevation (depending on spacing of hoops), respectively.

The “effective lateral stress” is approximated by

$$\sigma_2/f_{cc} = 0.5\,\alpha_n\alpha_s\omega_w \tag{8}$$

For the present cases where the unconfined concrete strength is 30 MPa, a comparison between the estimations using the above formulas, as well as the formulas proposed by Mander *et al.* (1988), and the numerical results is given in Table 3.

The numerical results generally agree with the predictions using the two simplified models, both in terms of the confining stress and the achieved axial compressive strength. The strength increase in the circular column, however, tends to be slightly underestimated in the numerical results (37.2 MPa as compared to 41.1 and 39.3 using CEB and Mander’s models, respectively).

It should be noted that the numerical modelling results presented and discussed in this paper have been focused on the strength of the confined concrete, as this is the most objective and stable parameter to be compared with the experimental data. As a matter of fact, the enhancement in the confined concrete in terms of ductility, including the slope of the softening branch and the ultimate strain, is equally important, especially in the design against extreme deformation such as in the

Table 3 Comparison of lateral confining effects with CEB and Mander *et al.* models

(all units in MPa)		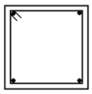	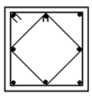	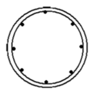
CEB FIP 1990 (1993)	$\sigma_2(=\sigma_x=\sigma_y)$	0.41	1.56	2.21
	f'_{cc}	32.1	37.8	41.1
Mander *et al.* (1988)	σ_2	1.24	1.28	1.53
	f'_{cc}	37.5	37.8	39.3
Numberical results	$\sigma_{x,y}$ (average)	0.66	1.24	1.72
	f'_{cc}	35.3	36.1	37.2

seismic resistant design. A reliable quantification of the ductility enhancement in a numerical analysis will depend more sensitively upon the soundness of the concrete material model in the softening phase, which in turn involves the considerations of localization and fracture energy. These modelling considerations will be investigated in the future study.

7. An illustrative example of confined concrete under dynamic compression

As stated earlier, one of the advantages of the current numerical model for steel-confined concrete, developed within a transient dynamic analysis code, is its easy extension to the analysis of confined concrete and its interaction with the reinforcing bars under a dynamic loading condition. In this section, an illustrative dynamic analysis example is given.

The short column with a rectangular transverse reinforcement is chosen to perform the dynamic analysis. A rapid compressive load, corresponding to a strain rate of about 1.0/s, is applied from the top of the column. The bottom is assumed to be a fixed boundary. This dynamic loading condition may be regarded as resembling the kind of dynamic load that may be experienced in RC piles driven by impact. As observed in the installation of such piles, the stress wave propagation and reflection within the pile due to the driving action can cause stress concentrations and stress reversals, which can be particularly damaging to the end regions of the pile (Thambiratnam 1990).

Fig. 14 shows the overall damage contour in the concrete, and the plastic strain distribution along the longitudinal rebar. It can be observed that under such a loading rate, a globally non-uniform distribution of the stress and the damage along the length of the column is developed. Dynamic failure occurs in the top region of the column, including within the confined concrete. Moreover, the longitudinal rebar is found to exhibit local yielding (buckling) near the impact end of the column. Examination of the detailed stress-strain response reveals that this local buckling occurs after the peak strength of the concrete is reached. Thus, the local buckling may be attributed to the combined effect of the transient stress wave and the reduced lateral constraint due to the damage/failure of the surrounding concrete.

To more realistically simulate the pile driven problem would require a comprehensive model

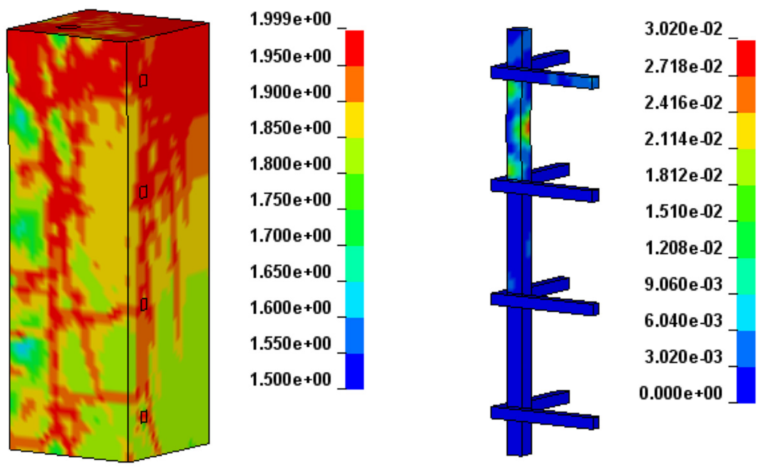

Fig. 14 Damage (left) and plastic strain (right) in concrete and confining steel

configuration taking into consideration of the soil conditions and the impact parameters. Once these conditions are defined, modification of the current model to suit such an analysis is rather straightforward. Extension to other dynamic problems involving confined concrete can be made in a similar way.

8. Conclusions

A numerical model for the analysis of concrete confined by transverse (and longitudinal) reinforcement is presented, along with a framework for a comprehensive evaluation of the numerical results concerning the underlying mechanisms in the development of the confinement effect. The computational model is developed using a general-purpose transient dynamic analysis code, and the material constitutive models employed have pressure and strain-rate sensitive features. Therefore, the model can be applied for the analysis under any arbitrary reinforcement and loading conditions, including dynamic loading. Such a model can also facilitate high fidelity numerical experiments which may be employed to complement physical tests and allow for a detailed examination of the underlying mechanisms.

Within the present paper, the model is applied for the analysis of axially loaded RC short columns under static loading, for validation and characterisation of the model performances. Three different transverse reinforcement configurations are considered. Results demonstrate that the numerical model is capable of reproducing the experimentally observed axial stress-strain characteristics for similar specimens. The strength enhancement ratios agree favourably with the experimental data and empirical predictions.

The numerical results enable a comprehensive securitization of the development of the confining stresses and how this correlates with the behaviour in the axial direction, including the attainment of the peak strength and the softening of the confined concrete core. Three distinctive stages, both for the confining stress and the stress in the transverse reinforcement, are identified based on the numerical results.

The numerical model has been constructed using a general purpose transient dynamic analysis code (LS-DYNA), and therefore it allows for a straightforward extension to low and high dynamic loading conditions, as well as analysis for complex loading combinations such as eccentric axial loading and bending. The potential influence of the material heterogeneity may be explored using a similar finite element framework but with a mesoscale setting, which will be the subject of a follow-up study.

References

Bazant, Z.P. and Oh, B.H. (1983), "Crack band theory for fracture of concrete", *Mater. Struct. (RILEM, Paris),* **16**, 155-177.

CEB-FIP Model Code 1990 (1993), Comite Euro-International du Beton, Redwood Books, Trowbridge, Wiltshire, UK.

Faria, R., Pouca, N.V. and Delgado, R. (2004), "Simulation of the cyclic behaviour of R/C rectangular hollow section bridge piers via a detailed numerical model", *J. Earthq. Eng.*, **8**(5), 725-748.

Foster, S.J., Liu, J. and Sheikh, S.A. (1998), "Cover spalling in HSC columns loaded in concentric compression", *J. Struct. Eng. - ASCE,* **124**(12), 1431-1437.

Kent, D.C. and Park, R. (1971), "Flexural members with confined concrete", *J. Struct. Div. - ASCE,* **97**(7), 169-1990.
Kwon, M. and Spacone, E. (2002), "Three-dimensional analysis of reinforced concrete columns", *Comput. Struct.*, **80**(2), 199-212.
Liu, J. and Foster, S.J. (2000), "A three-dimensional finite element model for confined concrete structures", *Comput. Struct*., **77**(5), 441-451.
LS-DYNA (2007), *Keyword user's manual*, Version 971, Livermore Software Technology Corporation.
Malvar, L.J., Crawford, J.E. and Morrill, K.B. (1999), "K&C concrete material model, release III: automated generation of material model input", *Rep. TR-99-24*, Karagozian & Case Structural Engineers, Burbank, Calif.
Malvar, L.J., Crawford, J.E., Wesevich, J.W. and Simons, D. (1997), "A plasticity concrete material model for DYNA3D", *Int. J. Impact Eng*., **19**(9/10), 847-873.
Mander, J.B., Priestley, M.J.N. and Park, R. (1988), "Theoretical stress-strain model for confined concrete", *J Struct. Eng*, **114**(8), 1804-1826.
Papanikolaou, V.K. and Kappos, A.J. (2009), "Numerical study of confinement effectiveness in solid and hollow reinforced concrete bridge piers: methodology", *Comput. Struct.*, **87**, 1427-1439.
Park, R., Priestley, M.J.N. and Gill, W.D. (1982), "Ductility of square confined concrete columns", *J. Struct. Eng.*, **108**(4), 929-950.
Saatcioglu, M. and Razvi, S.R. (1992), "Strength and ductility of confined concrete", *J. Struct. Eng.*, **118**(6), 1590-1607.
Scott, B.D., Park, R. and Priestley, M.J.N. (1982), "Stress-strain behaviour of concrete confined by overlapping hoops at high and low strain rates", *ACI J*., **79**(1), 13-27.
Sheikh, S.A. and Uzumeri, S.M. (1980), "Strength and ductility of tied concrete columns", *J. Struct. Div.*, **106**(ST5), 1079-1102.
Sheikh, S.A. and Uzumeri, S.M. (1982), "Analytical model for concrete confinement in tied columns", *J. Struct. Div.*, **108**(ST12), 2703-2722.
Thambiratnam, D.P. (1990), "Computer analysis of stress waves in driven piles", *Comput. Struct.*, **36**(4), 691-699.
Tu, Z.G. and Lu, Y. (2009), "Evaluation of typical concrete material models used in hydrocodes for high dynamic response simulations", *Int. J. Impact Eng.,* **36**(1), 132-146.